A reduced graphene oxide based electrochemical biosensor for tyrosine detection

2012 Nanotechnology 23 335707

(http://iopscience.iop.org/0957-4484/23/33/335707)

Nanotechnology **23** (2012) 335707 (7pp) doi:10.1088/0957-4484/23/33/335707

A reduced graphene oxide based electrochemical biosensor for tyrosine detection

Junhua Wei[1], Jingjing Qiu[1], Li Li[2], Liqiang Ren[2], Xianwen Zhang[1], Jharna Chaudhuri[1] and Shiren Wang[2]

[1] Department of Mechanical Engineering, Texas Tech University, 2500 Broadway, PO Box 41021, Lubbock, TX 79409-1021, USA
[2] Department of Industrial Engineering, Texas Tech University, 2500 Broadway, PO Box 43061 Lubbock, TX 79409-3061, USA

E-mail: Jenny.Qiu@ttu.edu and Shiren.Wang@ttu.edu

Received 31 May 2012, in final form 16 July 2012
Published 3 August 2012
Online at stacks.iop.org/Nano/23/335707

Abstract
In this paper, a 'green' and safe hydrothermal method has been used to reduce graphene oxide and produce hemin modified graphene nanosheet (HGN) based electrochemical biosensors for the determination of L-tyrosine levels. The as-fabricated HGN biosensors were characterized by UV–visible absorption spectra, fluorescence spectra, Fourier transform infrared spectroscopy (FTIR) spectra and thermogravimetric analysis (TGA). The experimental results indicated that hemin was successfully immobilized on the reduced graphene oxide nanosheet (rGO) through π–π interaction. TEM images and EDX results further confirmed the attachment of hemin on the rGO nanosheet. Cyclic voltammetry tests were carried out for the bare glass carbon electrode (GCE), the rGO electrode (rGO/GCE), and the hemin–rGO electrode (HGN/GCE). The HGN/GCE based biosensor exhibits a tyrosine detection linear range from 5×10^{-7} M to 2×10^{-5} M with a detection limitation of 7.5×10^{-8} M at a signal-to-noise ratio of 3. The sensitivity of this biosensor is 133 times higher than that of the bare GCE. In comparison with other works, electroactive biosensors are easily fabricated, easily controlled and cost-effective. Moreover, the hemin–rGO based biosensors demonstrate higher stability, a broader detection linear range and better detection sensitivity. Study of the oxidation scheme reveals that the rGO enhances the electron transfer between the electrode and the hemin, and the existence of hemin groups effectively electrocatalyzes the oxidation of tyrosine. This study contributes to a widespread clinical application of nanomaterial based biosensor devices with a broader detection linear range, improved stability, enhanced sensitivity and reduced costs.

(Some figures may appear in colour only in the online journal)

1. Introduction

Tyrosine (Tyr, or 4-hydroxyphenylalanine) is an aromatic amino acid that occurs in proteins for the regulation of signal transduction processes. Tyr is an important precursor of adrenaline, norepinephrine, dopamine, thyroid hormones, catecholamine, melanin and some estrogen [1]. It is used to establish and maintain the balance of nutrition for humans [2]. A deficiency of Tyr can induce diseases like hypochondria, dementia, hypothyroidism or Parkinson's [3, 4] while an excessive level of Tyr often leads to hyperthyroidism and sister chromatid exchange [5]. Therefore, an efficient determination of Tyr levels is critical in the diagnosis and treatment of diseases.

Several techniques have been used to test Tyr levels in the last few decades, including high performance

liquid chromatography (HPLC) [6], chromatography–mass spectrometry [7, 8] and capillary electrophoresis [9, 10]. However, the slow response, the expensive assays and the high equipment costs of these techniques have significantly impeded their wide application. Some other approaches have also attempted to measure Tyr levels, such as enzyme based methods [11] and fluorimetry [12]. However, these approaches suffer from either an unstable reagent or time-consuming preparation/measurement. Accordingly, there is a need to develop more efficient and reliable biosensors for determination of Tyr levels with high sensitivity and reduced cost.

In comparison with the above-mentioned conventional techniques, electrochemical detection of tyrosine is generally simple, rapid and stable [13]. With rapid advances in nanotechnology, nanomaterial based electrochemical biosensors have been intensively investigated. Diverse nanomaterials have been integrated into the electrodes for detection of diverse biomolecules on miniaturized devices [14–18]. Several carbon nanotube (CNT) based electrochemical biosensors have been developed to detect Tyr via the oxidation process. For example, Xu *et al* [19] presented the voltammetric responses of Tyr on multiwalled carbon nanotube (MWNT) electrodes. Liu *et al* [20] applied MWNT–ionic-liquid composite electrodes for Tyr detection. In addition, Ma *et al* [13] explored the testing of Tyr levels through immobilization of hemin onto poly(amidoamine)/MWNT nanocomposite film electrodes. Although these methods perform quickly and accurately in detection, the preparation and modification methods for the electrodes are complex and the detection linear ranges are rather limited (usually lower than 2×10^{-4} M). In contrast, some pregnant woman with PKU may have tyrosine concentrations even higher than 2×10^{-4} M [21]. Therefore, the limited detection linear ranges have significantly impeded their wide clinical applications.

Graphene is a one-atom-thick two-dimensional graphite carbon nanostructure [22, 23]. Owing to its large specific surface area and extraordinary electrical conductivity, graphene demonstrates great potential in biomedical and energy applications [24]. It is intensively investigated to work as a modification material on GC electrodes and graphite electrodes in novel electrochemical biosensors. Several efforts have been made to detect important biomolecules such as tripropylamine [25], dopamine [26], morphine [27] and DNA [28] using graphene based electrodes. Among these efforts, the technique of immobilizing hemin on graphene through aromatic π–π interaction [26, 28] was found to be very promising due to its enhanced electron transfer, enhanced electrostatic interaction, excellent electrocatalytic response, peroxidase-like activity and easy preparation. However, hydrazine, an unstable and toxic reagent, is demanded for the chemical reduction method [29, 30] during the preparation of graphene based conjugates.

In this paper, a hydrothermal method was used as a safe and green chemistry route for the reduction of graphene oxide. Hemin modified graphene nanosheet electrodes were successfully prepared in novel electrochemical biosensors for determining L-tyrosine levels. The electrocatalysis and electrical conductivity increased electron transfer for the L-tyrosine oxidization process. In comparison with other works, the resultant electrochemical biosensors demonstrated a broader detection range, better detection sensitivity, higher stability and outstanding reproducibility with significantly reduced cost. Moreover, the hydrothermal-treated biosensors are green, stable, easily fabricated, easily controlled and cost-effective in long-term use.

2. Experiment

2.1. Materials and reagents

Hemin (iron-containing porphyrin), from Sigma-Aldrich Inc., is the active center for a variety of proteins such as cytochromes, peroxidase, myoglobin and hemoglobin. It has been used in electrochemical detection due to its good electrocatalysis in the reversible redox of Fe(III)/Fe(IV). 0.2 M phosphate buffered saline (PBS, pH 7.0) was prepared from a certain concentration of potassium chloride, sodium chloride, disodium phosphate and monosodium phosphate. Ammonia, sodium chlorate, nitric acid and hydrochloric acid were obtained from Fisher Scientific Inc. L-tyrosine was purchased from Sigma-Aldrich Inc.

2.2. Chemical synthesis and electrode preparation

2.2.1. Synthesis of homogeneous graphene oxide solution. Graphite oxide was prepared by a modified Brodie method [32]. 10 g of graphite (provided by Asbury Carbons, NJ) was mixed with 160 ml of nitric acid and 85 g of sodium chlorate at room temperature. The mixture was stirred for 24 h. In order to remove the acidic and saline impurities, five cycles of hydrochloric acid and seven cycles of distilled water were used in rinsing the mixture. The graphene oxide film was achieved by drying in an oven at 70 °C. This film was then dispersed into distilled water by ultrasonication for 1 h to form a stable solution. This solution was centrifuged at 6000 rpm for 30 min. The upper homogeneous graphene oxide solution was collected.

2.2.2. Synthesis of HGN and pure rGO solution. The hemin–rGO (HGN) solution was synthesized by a hydrothermal method [31, 33] as follows: 40 ml of 0.5 mg ml^{-1} graphene oxide homogeneous solution was mixed with 10 ml of 1 mg ml^{-1} hemin solution (pH 10.5 adjusted by ammonia solution). Subsequently, the mixture was transferred into a 50 ml Teflon-lined autoclave and maintained at 180 °C for 12 h. The autoclave was then naturally cooled to room temperature, and the solution was vacuum filtrated through a 220 nm nylon paper to form a solid film. The final HGN solution was prepared by dispersing the solid film in PBS to form a 1 mg ml^{-1} solution. The rGO solution was prepared by a similar method without the addition of hemin solution. In comparison with the chemical reduction method using hydrazine, the presented hydrothermal method results in more stable π–π interactions in the resultant HGN. Moreover, the hydrothermal reduction is easy and nontoxic.

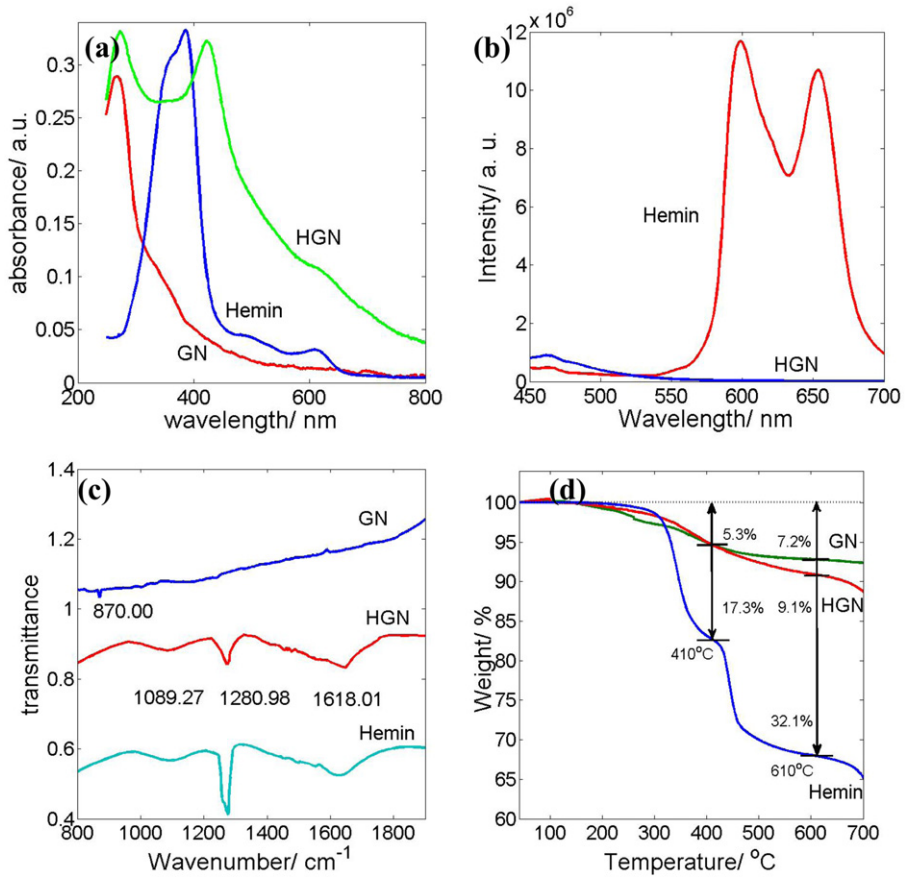

Figure 1. (a) UV–vis spectra of rGO, hemin and HGN solutions; (b) fluorescence spectra of hemin and HGN solutions; (c) FTIR transmittance results for rGO, hemin and HGN; (d) TGA results for rGO, hemin and HGN powders.

2.2.3. Electrode preparation and modification. The glassy carbon electrode (GCE) was first polished with alumina slurry, rinsed thoroughly with DI water and dried in air. 4 μl of the rGO and HGN solutions were dropped onto the surface of the GCE, respectively. They were both dried in a 70 °C oven for 10 min. Finally, the modified electrodes were activated with a 100 mV s^{-1} scan rate in a N_2-saturated 0.2 M PBS.

2.3. Apparatus and material characterization

In order to validate the successful attachment of hemin on the surface of the rGO nanosheet, UV–vis absorption spectra were recorded on a LAMBDA 1050 from PerkinElmer. TGA testing was carried out from 40 to 700 °C at a heating rate of 10 °C min^{-1} in N_2 atmosphere on a TGA Q90 (from TA). The fluorescence spectrum was measured with a FluoroMax-3. FTIR characterization was conducted by a JR100 FTIR spectrometer from Thermo Scientific. Moreover, transmission electron microscopy (TEM) images and energy-dispersive x-ray spectroscopy (EDX) were acquired on a Hitachi 8100 (operating at 75 kV). Electrochemical measurements were carried out on an electrochemical working station (CHI 660D, CH Instrument Inc.) with a three-electrode system including a 3 mm modified glassy carbon electrode (GCE) as the working electrode. A platinum (Pt) wire and KCl saturated Ag/AgCl were employed as the counter electrode and reference electrode.

3. Results and discussion

3.1. The characteristics of HGN

As shown in figure 1(a), the UV–visible absorption spectra of hemin, rGO and HGN in the water solution were compared. The spectrum of the hemin solution shows a strong Soret band peak and a shoulder band at around 380 nm. These peaks indicate the presence of a mixture of the dimer of hemin connected by μ-oxo bridges (minority) at 350 nm and the monomeric hemin hydroxide (majority) at 386 nm [33]. After reduction, the rGO solution shows a broad peak at 265 nm. Compared with the hemin and rGO solutions, the HGN solution exhibits major peaks at 265 nm and 420 nm without a shoulder peak. The 265 nm peak is consistent with the rGO solution and represents rGO after reduction. The 420 nm peak corresponds to the Soret band of hemin with a bathochromic shift (34 nm). This is attributed to the π–π aromatic interaction between hemin and rGO [28]. No shoulder peak exists around the 420 nm peak, which indicates the break of μ-oxo bridges during the reduction process. It is the monomeric hemin that participates in the π–π interaction.

Moreover, fluorescence spectra of the hemin and HGN solutions were acquired to demonstrate the electron transfer between hemin and rGO, as shown in figure 1(b). The influence of Fe^{3+} was removed by treating the hemin solution

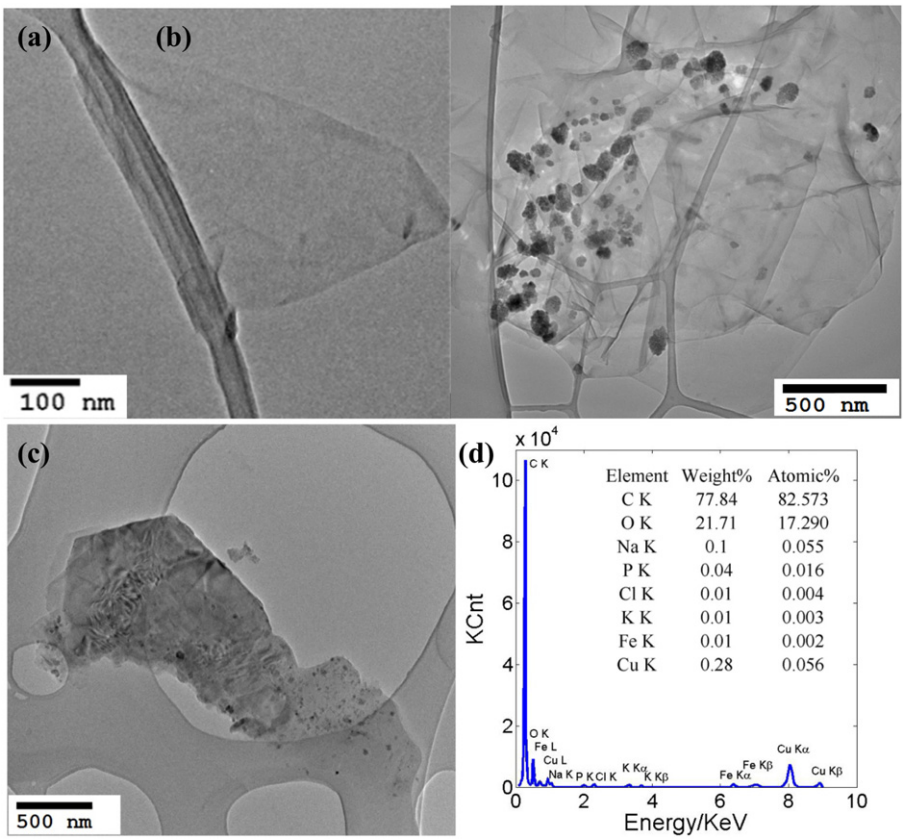

Figure 2. TEM images of (a) rGO and (b) and (c) HGN, and (d) the EDX result for HGN in (b).

with concentrated sulfuric acid. Using 400 nm excitation, a double peak can be observed from the pure hemin solution in the fluorescence emission spectrum. In comparison, no peak appears in the fluorescence emission spectrum of HGN. This quenching efficiency proves a good electron transfer between the hemin and the rGO.

FTIR characterization of the rGO, HGN and hemin was also carried out, as shown in figure 1(c). In the spectrum of hemin, the peak observed at 1280.98 cm^{-1} corresponds to C–O stretching vibration of the carboxyl group. The peak at 1618.01 cm^{-1} is assigned to the C=O stretching vibration of –NHCO–(amide I) [34]. Similarly, the spectrum of HGN shares the C–O and C=O characteristic peaks with hemin. In contrast to pure hemin and HGN, the peaks at 1618.01 and 1280.98 cm^{-1} vanished in the spectrum of rGO, which demonstrates that most oxygen-containing groups were effectively removed by the hydrothermal reduction method. The UV–visible, fluorescence spectra and FTIR spectra results demonstrate that hemin was successfully immobilized on rGO.

In addition, the thermal stability of rGO, hemin and HGN were evaluated by TGA. As shown in figure 1(d), all the samples were heated from room temperature to 700 °C. The TGA curve of pure hemin exhibits two stages: from room temperature to 410 °C and from 410 to 610 °C. For the first stage, hemin lost 17.3% of its weight, while HGN and rGO lost 5.3%. For the second stage, 32.1% of total weight was lost for hemin, compared with 7.2% and 9.1% weight loss for rGO and HGN, respectively. For HGN, the first stage could be mainly due to the slight decomposition of the rGO. The second stage could be due to the decomposition of hemin. This result further confirmed that the existence of hemin molecules on the surface of the rGO.

The morphology of HGN was characterized by TEM. Figure 2(a) illustrates the single-layer rGO. Although small hemin particles could not be seen obviously under TEM, figures 2(b) and (c) demonstrate that aggregated hemin particles were successfully attached on the rGO. The hemin aggregated into large particles because hemin is soluble in diluted ammonia but not water [35]. During transferral of the solutions into an autoclave, the hemin solution was diluted from pH 10.5 to pH 10.0. The decrease of pH value might influence the solubility of hemin. The elements of the materials in figure 2(b) were further investigated by EDX. As confirmed in figure 2(d), a small amount of Fe was found on the grid, which represents the existence of hemin on the surface of the rGO, while most of the C, Cu and O came from the carbon coated holey grid and the Na, K, Cl and P were most likely contributed by the PBS solution.

3.2. The electrochemical characteristics of the HGN/GC electrode

The attachment of immobilized hemin onto rGO was also demonstrated by an electrochemical method. Figure 3(a) shows the cyclic voltammetric (CV) curves recorded for

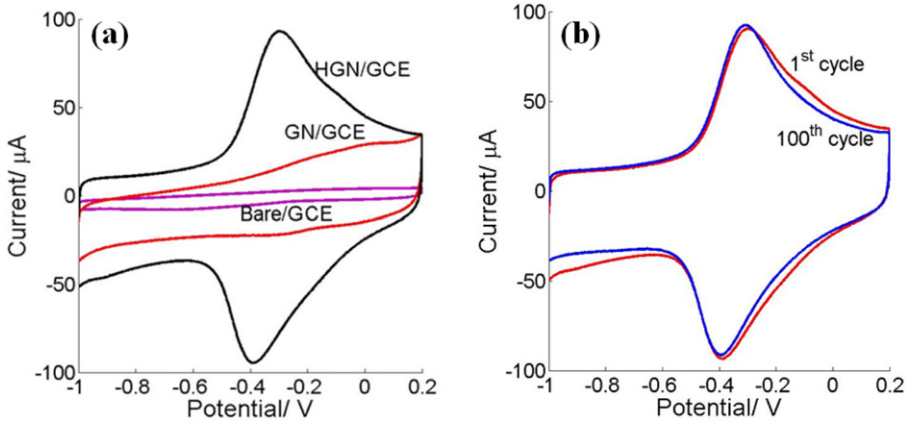

Figure 3. (a) CV test for the bare GCE, the RGO/GCE and the HGN/GCE, and (b) the first and 100th cycles of CV tests for the HGN/GCE in 0.2 M PBS (pH 7.0) with N_2 saturated at a scan rate of 100 mV s^{-1}.

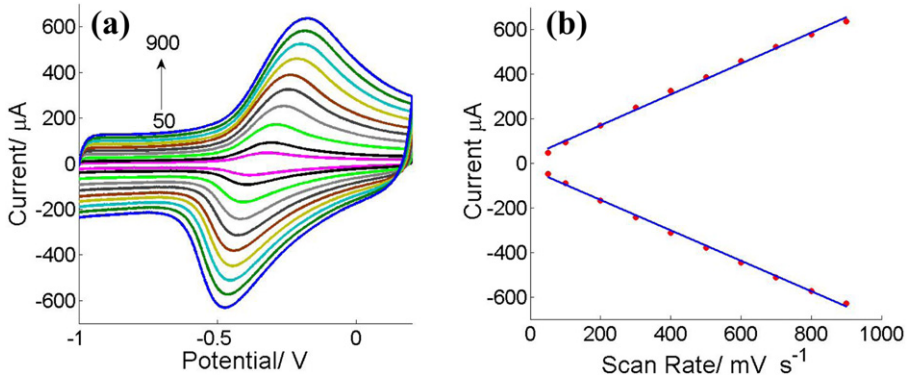

Figure 4. (a) CV of the HGN/GCE at rates of 50, 100, 200, 300, 400, 500, 600, 700, 800 and 900 mV s^{-1}, and (b) peak currents versus scan rate corresponding with (a).

bare GCE, rGO/GCE and HGN/GCE in 0.2 M pH 7.0 N_2-saturated PBS at a 100 mV s^{-1} scan rate. All the CV curves were recorded after several cycles of the CV when it became stable. No peak and only a very small current were recorded from the bare GCE. Compared with the bare GCE, the CV of the RGO/GCE shows a strong current due to the electronic double-layer capacitance of rGO. The CV of the HGN/GCE not only exhibits a strong capacitive current like the rGO/GCE, but also two well-defined quasi-reversible redox peaks which are ascribed to the electron transfer between the electrode and the redox center at the hemin. In addition, this curve presents an anodic peak potential (E_{pa}) at −0.299 V and a cathodic peak potential (E_{pc}) at −0.390 V with 91 mV peak potential separation (ΔE_p). The formal potential ($E^{o'}$ is the average value of E_{pa} and E_{pc}) was estimated at −0.34 V versus Ag/AgCl in saturated KCl solution. The peak anodic (i_{pa}) and cathodic (i_{pc}) currents were 58.2 μA and 60.2 μA. Figure 3(b) demonstrates the stability and reproducibility of the HGN/GCE electrochemical biosensor. Although slightly shifted (2.0%), the first cycle and the 100th cycle share the same peak potential separation, equal peak current and consistent formal potential. This result demonstrates that the electrochemistry of HGN/GCE has a good stability and reproducibility.

Furthermore, the influence of the scan rate on the CV curves of the HGN/GCE was also investigated. As shown in figure 4(a), the redox peak increase corresponds with the scan rate increase. The peaks for anodic current and cathodic current shift apart, while the formal potential stays still.

In addition, figure 4(b) plots the peak currents of the anode and the cathode versus the scan rate. From 50 to 900 mV s^{-1}, the peak currents vary linearly. The peak currents can be fitted by the following linear regression equations:

$$i_{pa} = 30.852 + 0.6952\nu, \qquad R_{pa} = 0.9981, \qquad (1)$$

$$i_{pc} = -27.781 - 0.6848\nu, \qquad R_{pc} = 0.9989, \qquad (2)$$

where ν is the scan rate, R denotes the linear correlation coefficient and i_{pa} and i_{pc} are the currents at peak in the anodic and cathodic curves, respectively. This is in accordance with the equation $i_p = nFQ\nu/4RT$ [13] (where Q is the charge consumed in Coulombs, F is the Faraday constant, n is the number of the electrons transferred and the other terms have their standard meanings). These characteristics suggest that the redox reaction of the HGN/GCE is an equal-intensity, quasi-reversible and surface-controlled electrochemical process. All of the electrochemical characterization results validate that the hydrothermal method works well to produce a long-term stable HGN/GCE biosensor.

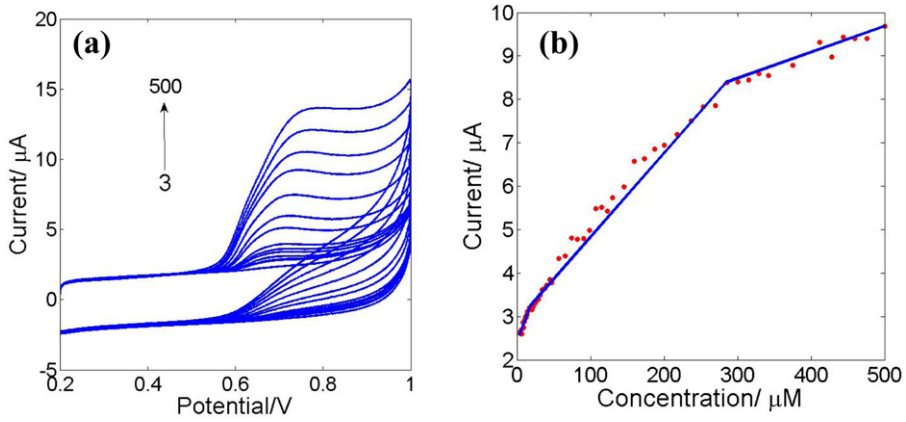

Figure 5. (a) Dependence of the peak current of Tyr on its concentration for Tyr concentrations of 3, 8, 13, 20, 32, 48, 91, 130, 200, 285, 375 and 500 μM (from bottom to top). (b) The anodic current at 6.4 V versus concentration of L-tyrosine corresponding with (a).

3.3. Electrocatalytic oxidation of L*-tyrosine at the HGN/GCE*

According to the literature [33], (OH)Fe^{+3}–P can be oxidized into O=Fe^{+4}–P by electrochemical oxidation where P represents porphyrin. In this paper, when a +0.64 V potential is present, (OH)Fe^{+3}–P is oxidized to O=Fe^{+4}–P. Subsequently, the L-tyrosine is radically oxidized by O=Fe^{+4}–P. Hemin effectively electrocatalyzes the oxidation process of L-tyrosine. As the graphene provides additional electrons as an outstanding electron conductor and favorable large specific area material, and hemin plays the role of a catalytic mediator for L-tyrosine oxidation, the HGN/GCE is promising as a highly sensitive L-tyrosine sensor.

Figure 5(a) records a series of CV with increasing Tyr concentration. Figure 5(b) shows the anodic current at 0.64 V versus Tyr concentration. According to figure 5(b), a linear range relationship is confirmed. The linear range of oxidation current versus Tyr concentration could be separated into three ranges: (i) 5×10^{-7} to 2×10^{-5} M, (ii) 2×10^{-5} to 3×10^{-4} M and (iii) 3×10^{-4} to 5×10^{-4} M. The corresponding regression equations for these ranges are

$$i_1 = 2.4252 + 0.044c_{\text{tyr}}, \qquad R_1 = 0.9630, \qquad (3)$$

$$i_2 = 2.8904 + 0.019c_{\text{tyr}}, \qquad R_2 = 0.9885, \qquad (4)$$

$$i_3 = 6.6900 + 0.006c_{\text{tyr}}, \qquad R_3 = 0.9668, \qquad (5)$$

where c_{tyr} represents the concentration of Tyr, i_n ($n = 1$, 2 or 3) is the current during the different n ranges. The detection limit was estimated to be 7.5×10^{-8} M at a signal to noise ratio of 3. Moreover, the sensitivity can be calculated to be 0.48 μA μM^{-1} cm^2 by the ratio of the slope in figure 5(b) and the electrode area of 0.09 cm^2.

In the first linear range, Tyr molecules are rarely in the solution. A single Tyr molecule will be oxidized directly when an anodic current is presented [13]. The oxidation scheme for the hemin–rGO based electrode is indicated in figure 6.

In this condition, the slope of current versus concentration represents a single Tyr molecule being oxidized by electrons. Compared with the first linear range, there are plenty of Tyr molecules in the PBS solution during the second linear range. This means that two Tyr molecules could easily form a dimer of Tyr after oxidation [36] as shown in the lower part of figure 6. In this case, the slope would drop to half of the first linear range (from 0.044 to 0.019) because this current represents the case where the electrons oxidize two Tyr molecules instead of one. The decrease of the slope suggests that either the quantity of electrons provided by the rGO becomes insufficient or the electrocatalytic ability of the hemin is nearly saturated as more Tyr is added. The slope zeroes during this process when the concentration of Tyr molecules exceeds the oxidation ability for this HGN/GCE sensor.

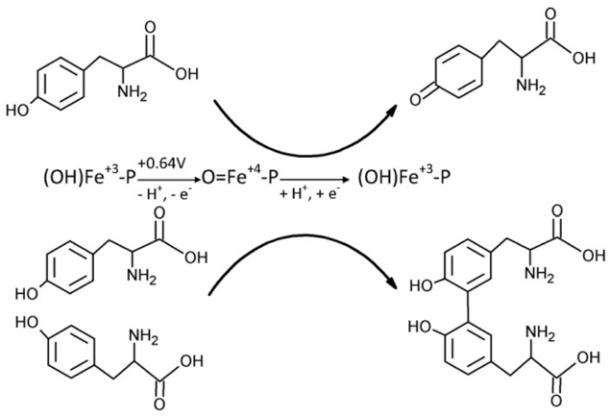

Figure 6. The tyrosine oxidation scheme for low concentration (top) and high concentration (bottom).

In addition, the biosensor performance in this work was compared with other electrochemical methods that have been reported, as shown in table 1. The table shows that this approach provides the largest linear range with a relatively low detection limit for Tyr detection. Since the π–π interaction between hemin and rGO is not limited by the amount of functional groups in covalent bonding, a relatively larger amount of hemin can be attached onto the rGO, which results in a relatively lower detection limit. The advantage of graphene nanosheets is utilized to improve the electron transfer efficiency and obtain a stable signal even for high

Table 1. Comparison of the performances of different L-tyrosine sensors.

Electrodes	Linear range ($\times 10^{-4}$ M)	Detection limit (M)	Reference
Bare GCE	0.1–2	1.0×10^{-5}	[37]
MWCNT/GCE	0.001–0.5	8.0×10^{-8}	[36]
L-serine polymer film/GCE	0.003–1	1.0×10^{-7}	[5]
SWCNT/GCE	0.05–0.2	9.0×10^{-8}	[38]
Hemin/PAMAM/MWCNT/GCE	0.001–0.29	1.0×10^{-8}	[13]
Hemin/rGO/GCE	0.005–5	7.5×10^{-8}	This work

Tyr concentrations. The above evidence indicates that the hemin–rGO prepared through the hydrothermal method is easier to use and more effective in the determination of L-tyrosine levels.

4. Conclusion

In this study, an easy and 'green' hydrothermal method of immobilizing hemin onto rGO was investigated. The hemin functionalized rGO was successfully employed to modify a glass carbon electrode for efficient detection of Tyr levels. The result indicates that rGO provides an outstanding platform for the immobilization of hemin. In the resultant biosensor, the rGO enhanced the electron transfer between the hemin and the electrode while the hemin catalyzed the L-tyrosine oxidization. This method provides the opportunity to achieve effective determination of Tyr levels on miniaturized devices and could be a better choice in the diagnosis and treatment of diseases for practical clinical use.

Acknowledgments

The authors gratefully acknowledge Dr Louisa J Hope-Weeks for her help with the fluorescence spectroscopy test. The authors would also like to thank Dr Brandon Weeks for his help with the UV–vis spectra characterization. The authors Xianwen Zhang and Jharna Chaudhuri acknowledge the support of the National Science Foundation (NSF) Grant No. MRI 0922898 for the HR-TEM work.

References

[1] Banderet L and Lieberman H 1989 *Brain Res. Bull.* **22** 759–62
[2] Resnick S I, Hernandez L, Chen J and Hoebel B G 1978 *Pharmacology* **3** 157–62
[3] Meyer J S, Welch K M, Deshmukh V D, Perez F I, Jacob R H, Haufrect D B, Mathew N T and Morrell R M 1977 *J. Am. Geriatr. Soc.* **25** 289–98
[4] Gelenberg A J, Gibson C J and Wojcik J D 1982 *Psychopharmacol. Bull.* **18** 7–18
[5] Li C 2006 *Colloids Surf.* B **50** 147–51
[6] Sabine L, Jean P G, Joelle S and Bernard B 1997 *J. Chromatogr.* B **696** 9–17
[7] Felitsyn N M, Henderson G N, James M O and Stacpoole P W 2004 *Clin. Chim. Acta* **250** 219–30
[8] Ishii Y, Lijima M, Umemura T, Nishikawa A, Iwasaki Y, Ito R, Saito K, Hirose M and Nakazawa H 2006 *J. Pharm. Biomed. Anal.* **41** 1325–31
[9] Huang Y, Jiang X, Wang W, Duan J P and Chen G N 2005 *Talanta* **70** 1157–63
[10] Latorre R M, Saurina J and Cassou S H 2000 *J. Chromatogr.* A **871** 331–40
[11] Rivas G A and Solis V M 1991 *Anal. Chem.* **63** 2762–5
[12] Wang F, Qing Y and Ci Y X 1992 *Anal. Lett.* **25** 1469–78
[13] Ma Q, Ai S, Yin H, Chen Q and Tang T 2010 *Electrochim. Acta* **55** 6687–94
[14] Le Floch F, Thauaire A, Bidan G and Simonato J P 2009 *Nanotechnology* **20** 145705
[15] Esplandiu M J, Pacios M, Cyganek L, Bartroli J and Del Valle M 2009 *Nanotechnology* **20** 355502
[16] El-Said W A, Kin T H, Kin H and Choi J W 2010 *Nanotechnology* **21** 455501
[17] Marin S and Merkoçi A 2009 *Nanotechnology* **20** 055101
[18] Asis E Jr, Leung J, Wood S and Nguyen C 2010 *Nanotechnology* **21** 125101
[19] Xu Q and Wang S F 2005 *Microchim. Acta* **151** 47–52
[20] Liu L Q, Zhao F Q, Xiao F and Zeng B Z 2008 *Electronanalysis* **20** 2148–52
[21] Spronsen F J V, Rijn M V, Bekhof J, Koch R and Smit P G A 2001 *Am. J. Clin. Nutr.* **73** 153–7
[22] Wang S and Qiu J 2011 *J. Appl. Polym. Sci.* **119** 3670–4
[23] Wang S, Zhang Y and Abidi N 2009 *Langmuir* **25** 11078–81
[24] Xu Y, Bai H, Lu G, Li C and Shi G 2008 *J. Am. Chem. Soc.* **130** 5856–7
[25] Yu Y, Zhou M, Shen W, Zhang H, Cao Q and Cui H 2012 *Carbon* **50** 2539–45
[26] Wu L, Feng J, Ren L and Qu X 2012 *Biosens. Bioelectron.* **34** 57–62
[27] Avaee A, Salimi A and Teymourian H 2012 *Biosens. Bioelectron.* **31** 205–11
[28] Guo Y, Deng L, Li J, Guo S, Wang E and Dong S 2011 *ACS Nano* **5** 1282–90
[29] Zhou Y, Bao Q, Tang L, Zhong Y and Loh K 2009 *Chem. Mater.* **21** 2950–6
[30] Chen J, Zhao L, Bai H and Shi G 2011 *J. Electroanal. Chem.* **657** 34–8
[31] Zhou Y, Bao Q L, Tang L A L, Zhong Y L and Loh K P 2009 *Chem. Mater.* **21** 2950–6
[32] Wang S, Tambraparni M, Qiu J, Tipton J and Dean D 2009 *Macromolecules* **42** 5251–5
[33] Silver J and Lukas B 1983 *Inorg. Chim. Acta* **78** 219–24
[34] Xu C, Li J, Wang X, Wang J, Wan L, Li Y, Zhang M, Shang X and Yang Y 2012 *Mater. Chem. Phys.* **132** 858–64
[35] Budavari S, O'Neil M, Smith A, Heckelman P and Obenchain J 1996 *Merck Index* 12th edn (CRC Press) pp 793–4
[36] Breydo L, Wu J W and Uversky V 2012 *Biochim. Biophys. Acta* **1822** 261–85
[37] Groves J and Gilbert J A 1986 *Inorg. Chem.* **25** 123–5
[38] Rivas G A and Solis V M 1991 *Anal. Chem.* **63** 2762–5